Three Velocity Component, Nonhomogeneous Atmospheric Boundary-Layer Turbulence Modeling

M. Perlmutter*
U.S. ERDA, Pittsburgh Energy Research Center, Pittsburgh, Pa.
W. Frost†
University of Tennessee Space Institute, Tullahoma, Tenn.
G. H. Fichtl‡
NASA Marshall Space Flight Center, Huntsville, Ala.

A new method of simulating the atmospheric turbulent winds by filtering Gaussian white noise signals and thereby generating signals that have the same second moment statistics as the atmospheric winds is presented. The governing equations are developed for the two-level autospectrum for the turbulent-wind components. A control system is modeled in which white Gaussian noise signals can be filtered, thereby generating signals with the same two level autospectra as the turbulent winds. An example calculation using the Dryden Autospectrum, an exponential coherence, and a linear phase angle is illustrated. The method is extended to include the two-level cross-spectrum between orthogonal components as well, and the appropriate filters are developed.

I. Introduction

THE present investigation reports a new model for simulating low-altitude wind turbulence. The model is based on filtering Gaussian random noise signals in such a manner that the output signals have the same statistical behavior as the low-altitude wind turbulence. This model is useful for several reasons. The model incorporates various statistical wind data such as spectra, coherence, and phase angle and pinpoints the type of wind data needed to refine, test, and improve simulation techniques.

Since the model gives a functional form of the turbulent wind components, various mathematical manipulations that generate other functions of interest such as wind derivates can be carried out. Also, since the model can be utilized to generate numerical wind signals, the wind interactions with various objects can numerically be evaluated. This allows solutions to complex nonlinear stochastic problems that could not be solved analytically.

The present analysis uses a number of Gaussian random white noise signals which are passed through lagging filters and shaping filters such that the three components of the model signal have the same statistical characteristics as the three turbulent wind components in a vertical plane. For instance, the correlations between the turbulent wind component at one arbitrary altitude with a turbulent wind component at some other altitude will be the same as the model signals generated for the two different altitudes.

A general discussion of methods for generating quasi-random signals that simulate physical random phenomena is given by Fichtl et al.[1] in Chapter 14. A report using a similar approach to the present method was first reported by Fichtl and Perlmutter.[2] Although the report was limited to one wind component, the present report extends the results to three turbulent wind components.

A very complete study of low-altitude wind statistics and their use in atmospheric modeling is given by Barr et al.[3] In their model, they discuss the wind simulation treated as a homogeneous process at one level. The one-level spectra are satisfied and the one-level wind components are obtained. To account for changes in altitude of the aircraft the parameters of the one level spectra are allowed to vary.

The present method differs from that in Ref. 3 in that it evaluates the entire turbulent field satisfying the correlation between wind components at different altitudes. This is not true in Ref. 3. The present method, however, does not require solving for the entire turbulent field. The turbulence winds can be evaluated in a region along the aircraft trajectory, thus giving the wind turbulence incident on the aircraft as a function of time.

In Ref. 4, the interlevel correlation was taken into account. The three components of velocity were evaluated at two different altitudes. The three wind components at the two different altitudes are treated as six separate signals with known autospectra for each signal and known cross-spectra between the signals. However, the present method is superior in that it solves for the entire field as a continuous function and is not limited to solving for specific signals at specific altitudes.

In the following analysis, we will simulate the three turbulent wind components in a vertical plane that contains the aircraft trajectory. The wind turbulence is a stochastic function of position but is not dependent on time. This is Taylor's frozen-turbulent-field hypothesis. This postulates that if an aircraft moves through a turbulent field at a sufficiently high rate of speed, the change of the turbulent components in time have a negligible effect on the statistical behavior of the wind incident on the aircraft. We can calculate the turbulent velocity components incident on the aircraft as a function of time as the aircraft passes through the turbulent field. Since the entire turbulent field in the plane is known in the present model, it is possible to solve for the turbulence incident on the aircraft as a function of time whatever its trajectory is in the vertical plane. We could similarly treat turbulent winds incident on structures by considering that the turbulence is being carried past the building by the mean wind.

In the following, we shall first derive the random wind statistics that must be satisfied by the model. We shall then model the three components assuming initially that the interlevel cross-spectra between orthogonal wind components can be neglected. This greatly simplifies the calculation since

Received June 28, 1976; presented as Paper 76-413 at the AIAA 9th Fluid and Plasma Dynamics Conference, San Diego, Calif., July 14-16, 1976; revision received July 11, 1977.

Index categories: Atmospheric and Space Sciences; Simulation; Computational Methods.

*Combustion Division.

†Director, Atmospheric Science Division.

‡Chief, Environment Dynamics Branch. Associate Fellow AIAA.

now each wind component can be modeled separately. This is also a reasonable assumption as discussed in Ref. 3. We then show that the functions that describe the frozen turbulent field can be transformed to the turbulent wind components incident on the aircraft as a function of time by using Taylor's hypothesis.

After describing some of the statistical data of atmospheric turbulence that has been obtained and is used in the model, some examples are carried out to illustrate the numerical techniques for generating the random signals and to show that the random signals do indeed have the appropriate spectral behavior. The results are then extended to include the case in which the cross-spectral quantities relating the orthogonal wind components are included in the simulation. The analysis of generating the wind signals for this case is carried out and finally an example case is given to illustrate that the proper spectral behavior is obtained for this case also. Details concerning some of the discussed points are given in Ref. 5.

II. Definition of Problem

A one-dimensional Fourier decomposition of the $u_i(x,y,z,t)$ component of turbulence along the x axis (directed along the mean wind vector) is given by

$$u_i(x,y,z,t) = \frac{1}{2\pi}\int_{-\infty}^{+\infty} \hat{u}_i(k,y,z,t)e^{ikx}\mathrm{d}k \tag{1}$$

where $\hat{u}_i(k,y,z,t)$ is the Fourier transform of $u(x,y,z,t)$ at the spatial frequency or wave number $k(\mathrm{rad}m^{-1})$. The inverse Fourier transform is given by

$$\hat{u}_i(k,y,z,t) = \int_{-\infty}^{+\infty} u_i(x,y,z,t)e^{-ikx}\mathrm{d}x \tag{2}$$

The y and z axes are orthogonal to the x axis with the z axis directed along the upward vertical. The turbulence energy spectrum has been assumed sufficiently continuous to avoid the use of the proper Fourier-Stieltjes integral form of Eq. (1) (see Ref. 1). Since we are presently concerned with the turbulence in the x-z plane at a given instant (frozen-field hypothesis), we will not carry the y and t along in this part of the analysis. Let us construct the correlation function by evaluating Eq. (1) at (x_1,z_1) and at $(x_1+r,z_1-\Delta_{12})$ as shown in Fig. 1. Multiplying and then averaging over the ensemble we obtain

$$\begin{aligned} R_{ij}(r,x,z_1,z_2) &= \langle u_i(x,z_1)u_j(x+r,z_2)\rangle \\ &= \frac{1}{2\pi}\int_{-\infty}^{+\infty}\langle u_i(k,z_1)\hat{u}_j^*(k',z_2)\rangle \\ &\quad\times\exp\{i[(k-k')x-k'r]\}\mathrm{d}k\mathrm{d}k' \end{aligned} \tag{3}$$

Note that when the subscripts are the same this does not assume the summation convention. Since the analysis is restricted to the case of a horizontally homogeneous turbulence process the cross-correlation of the Fourier amplitudes must depend only on r and therefore have the form

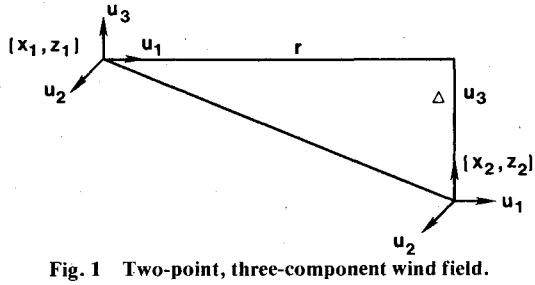

Fig. 1 Two-point, three-component wind field.

$$\langle \hat{u}_i(k,z_1)\hat{u}_j^*(k',z_2)\rangle = \phi_{ij}(k',z_1,z_2)\delta(k'-k) \tag{4}$$

where $\delta(k'-k)$ is the Dirac delta function and $\phi_{ij}(k',z_1,z_2)$ is the interlevel cross-spectrum. Combining the above then gives

$$R_{ij}(r,z_1,z_2) = \frac{1}{2\pi}\int_{-\infty}^{\infty}\phi_{ij}(k,z_1,z_2)e^{ikr}\mathrm{d}k \tag{5}$$

We can express ϕ_{ij} in terms of a real and imaginary part

$$\phi_{ij} = C_{ij} - i\,Q_{ij} \tag{6}$$

where the real part, C_{ij}, is called the coincident spectrum or cospectrum and the imaginary part, Q_{ij}, is called the quadrature spectrum or quadspectrum.[6]

The ϕ_{ij} can also be specified in terms of the nondimensional magnitude called the coherence coh_{ij} and phase angle θ_{ij} namely

$$\mathrm{coh}_{ij}(k,z_1,z_2) = \frac{\phi_{ij}(k,z_1,z_2)\phi_{ij}^*(k,z_1,z_2)}{\phi_{ii}(k,z_1,z_1)\phi_{jj}(k,z_2,z_2)} \tag{7a}$$

$$\theta_{ij}(k,z_1,z_2) = \tan^{-1}\frac{Q_{ij}(k,z_1,z_2)}{C_{ij}(k,z_1,z_2)} \tag{7b}$$

where * denotes the complex conjugate so that

$$\begin{aligned} \phi_{ij}(k,z_1,z_2) &= [\phi_{ii}(k,z_1,z_1)\phi_{jj}(k,z_2,z_2) \\ &\quad\times\mathrm{coh}_{ij}(k,z_1,z_2)]^{1/2}\exp[-i\theta_{ij}(k,z_1,z_2)] \end{aligned} \tag{8}$$

where $\phi_{ij}(k,z,z)$ is the one-level spectrum. Thus specification of the functions $\phi_{ii}(k,z_1,z_1)$, $\phi_{jj}(k,z_2,z_2)$, $\mathrm{coh}_{ij}(k,z_1,z_2)$, and $\theta_{ij}(k,z_1,z_2)$ where i,j have values 1, 2, 3 serves to completely specify the function $\phi_{ij}(k,z_1,z_2)$ and hence the second moment statistics of $u_i(x,z)$. In the development that follows we seek a filter such that upon input of white noise signals an output $v_i(x,z)$ that possesses second moment statistics similar to the signal $u_i(x,z)$ will result.

III. Synthesis for Uncorrelated Components

Consider first the case where the cross correlations between orthogonal wind components can be neglected. According to

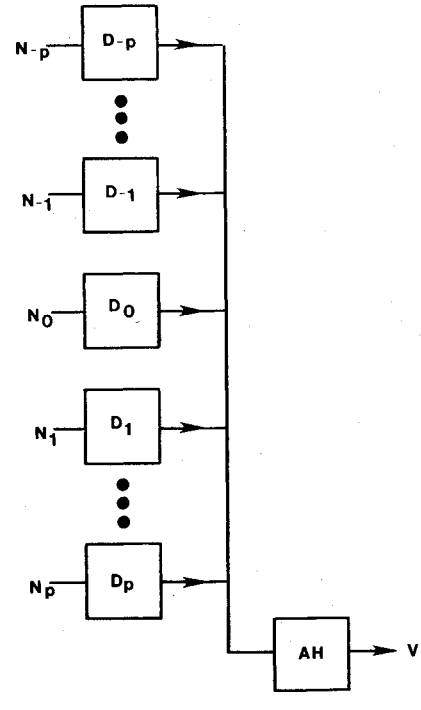

Fig. 2 Control system model.

Ref. 3 this is a reasonable assumption, as will be discussed later. (The method of including the cross correlation when necessary will also be discussed later.) When the cross correlation between orthogonal wind components can be neglected, then each wind component is modeled separately with independently generated input signals so that the different wind components are uncorrelated. The model output v_i is generated to have the same statistics as the wind component u_i. That is, the simulated wind v_i satisfies the appropriate power spectrum, coherence, and phase angle over the range of altitudes z for which we wish to simulate the turbulent field. Since each component can be generated separately for simplicity the subscript on v will be suppressed in order to simplify the nomenclature.

The one-dimensional Fourier decomposition of the random process field $v(x,z)$ is given as before by

$$v(x,z)=\frac{1}{2\pi}\int_{\infty}^{\infty}\hat{v}(k,z)e^{ikx}\mathrm{d}k \tag{9}$$

The control system model with which we plan to simulate the wind turbulence u_i is shown in Fig. 2. There are several independent horizontally homogeneous Gaussian white noise sources, the Fourier transform of the ℓth white noise process being $\hat{N}_\ell(k)$. This ℓth noise passes through lag filters D_ℓ and the output is summed over the noises to give a composite process $v_c(k,z)$. The composite process $v_c(k,z)$ then passes through a shaping filter $A\hat{H}(k,z)$ to obtain the process $v(x,z)$. Thus we can write

$$\hat{v}(k,z)=A\hat{H}(k,z)\sum_{\ell=-p}^{p}D_\ell(k,z)\hat{N}_\ell(k) \tag{10}$$

where A is a constant multiplier that will be specified later.

Hence using several independent white Gaussian noises passed through filters we can obtain the signal v which is to have the same statistical characteristics as u. Multiplying Eq. (10) by its complex conjugate evaluated at k' and z_2 and ensemble averaging we obtain

$$\langle\hat{v}(k,z_1)\hat{v}^*(k',z_2)\rangle=A^2\hat{H}(k,z_1)\hat{H}^*(k',z_2)\times\sum_{\ell=-p}^{p}\sum_{m=-p}^{p}D_\ell(k,z_1)D_m^*(k',z_2)\langle\hat{N}_\ell(k)\hat{N}_m^*(k')\rangle \tag{11}$$

White noise processes are statistically independent and their Fourier transforms are orthogonal with unit spectral density, hence

$$\langle N_\ell(k)N_m^*(k')\rangle=\delta(k-k')\delta_{\ell m} \tag{12}$$

where $\delta_{\ell m}$ is the Kronecker delta. We can then write the model two point autospectrum $m\phi(k,z_1,z_2)$ as

$$m\phi(k,z_1,z_2)=A^2\hat{H}(k,z_1)\hat{H}^*(k,z_2)\sum_{m=-p}^{p}\times D_m(k,z_1)D_m^*(k,z_2)=A^2\phi_H(k,z_1,z_2)\phi_s(k,z_1,z_2) \tag{13}$$

where

$$\phi_H\equiv A^2HH^*\ \text{and}\ \phi_s\equiv\sum_{m=-p}^{p}D_mD_m^*$$

A. Coherence Matching

From Eqs. (7a) and (13) we can write the model coherence mcoh as

$$\mathrm{mcoh}(k,z_1,z_2)=\frac{m\phi(k,z_1,z_2)m\phi^*(k,z_1,z_2)}{m\phi(k,z_1,z_1)m\phi(k,z_2,z_2)}=\frac{A^4\phi_H(k,z_1,z_2)\phi_s(k,z_1,z_2)\phi_H^*(k,z_1,z_2)\phi_s^*(k,z_1,z_2)}{A^4\phi_H(k,z_1,z_1)\phi_s(k,z_1,z_1)\phi_H(k,z_2,z_2)\phi_s(k,z_2,z_2)} \tag{14}$$

Since

$$\frac{\phi_H(k,z_1,z_2)\phi_H^*(k,z_1,z_2)}{\phi_H(k,z_1,z_1)\phi_H(k,z_2,z_2)}=\frac{H(k,z_1)H^*(k,z_2)H^*(k,z_1)H(k,z_2)}{H(k,z_1)H^*(k,z_1)H(k,z_2)H^*(k,z_2)}=1$$

Equation (14) reduces to

$$\mathrm{mcoh}(k,z_1,z_2)=\frac{\left(\sum_{m=-p}^{p}D_m(k,z_1)D_m^*(k,z_2)\right)\left(\sum_{\ell=-p}^{p}D_\ell^*(k,z_1)D_\ell(k,z_2)\right)}{\left(\sum_{m=-p}^{p}D_m(k,z_1)D_m^*(k,z_1)\right)\left(\sum_{\ell=-p}^{p}D_\ell^*(k,z_2)D_\ell(k,z_2)\right)} \tag{15}$$

We shall now proceed to match the model coherence, one level autospectra, and phase angle to the turbulent wind values.

Note that the coherence is independent of $AH(k,z)$ and is only a function of the lag filters $D_m(k,z)$. The shaping filter $AH(k,z)$ will be reserved for autospectra and phase angle matching. Thus the functions $D_\ell(k,z)$ will be formulated so that the model coherence, mcoh, will be equal to the turbulent wind coherence, coh.

At this point, we shall specialize to a class of processes with coherence functions dependent on difference in altitude $\Delta_{12}=z_1-z_2$. The motivation for this is that the turbulence coherence near the ground ($z\le 150$ m) appears to behave as $\mathrm{coh}=\exp(-a|k\Delta|)$. This is given in Refs. 4 and 7. A method of satisfying an arbitrary coherence function can be formulated by assuming that $D_\ell(k,z)$ is a pure lead or lag. We can then write

$$D_\ell(k,z)=C_\ell e^{ikzd_\ell}\qquad D_{-\ell}(k,z)=C_\ell e^{-ikzd_\ell}$$
$$\ell=1,2,\ldots,p\qquad D_0(k,z)=C_0 \tag{16}$$

Then we obtain the result

$$\sum_{\ell=-p}^{+p}D_\ell(k,z_1)D_\ell^*(k,z_2)=C_0^2+\sum_{\ell=1}^{p}C_\ell^2(e^{-ik\Delta d_\ell}+e^{+ik\Delta d_\ell})=C_0^2+2\sum_{\ell=1}^{p}C_\ell^2\cos(k\Delta d_\ell) \tag{17}$$

Notice that C_ℓ and d_ℓ are equal for D_ℓ and $D_{-\ell}$. We similarly obtain the result

$$\sum_{\ell=-p}^{p}D_\ell^*(k,z_1)D_\ell(k,z_2)=C_0^2+2\sum_{\ell=1}^{p}C_\ell^2\cos(k\Delta d_\ell) \tag{18}$$

Thus we can see that

$$\mathrm{mcoh}(k,z_1,z_2)=\frac{\left(C_0^2+2\sum_{\ell=1}^{p}C_\ell^2\cos(k\Delta d_\ell)\right)^2}{\left(C_0^2+2\sum_{\ell=1}^{p}C_\ell^2\right)^2} \tag{19}$$

As mentioned previously, the commonly assumed form for the atmospheric coherence can be expressed as

$$\text{coh}(k\Delta) = e^{-a|k\Delta|} = e^{-a|\epsilon|} = e^{-a\epsilon_0|\xi|} = e^{-|\xi|/\xi_0} \tag{20}$$

where $\epsilon = k\Delta$, ϵ_0 is the maximum value of $k\Delta = \epsilon$, over which the coherence is significant and ξ is equal to ϵ/ϵ_0, whereas $\xi_0 = 1/a\epsilon_0$. The present analysis is not restricted to the exponential form of the coherence.

Equation (19) can now be written

$$\text{mcoh}^{1/2} = \sum_{\ell=0}^{p} \alpha_\ell \cos(\pi \ell \xi) \tag{21}$$

where

$$d_\ell = \pi \ell / \epsilon_0 \tag{22}$$

and

$$\alpha_0 = \frac{C_0^2}{s_p}, \quad \alpha_1 = \frac{2C_1^2}{s_p}, \quad \alpha_2 = \frac{2C_2^2}{s_p}, \ldots, \quad \alpha_p = \frac{2C_p^2}{s_p} \tag{23}$$

where

$$s_p = C_0^2 + 2\sum_{\ell=1}^{p} C_\ell^2 \tag{24}$$

To evaluate the values of C giving minimum error between the model coherence mcoh and the wind coherence coh, the error E can be written as

$$E = \int_0^1 [\text{mcoh}^{1/2}(\xi) - \text{coh}^{1/2}(\xi)]^2 d\xi \tag{25}$$

$$= \int_0^1 \left[\left(\sum_{\ell=0}^{p} \alpha_\ell \cos \pi \ell \xi\right) - \text{coh}^{1/2}(\xi)\right]^2 d\xi \tag{26}$$

Using orthogonality α_k', where α_ℓ' refers to the values of α_ℓ that will minimize the error E, can be found as

$$\alpha_k' = 2\int_0^1 \text{coh}^{1/2}(\xi) \cos(k\pi\xi) d\xi \qquad k \neq 0$$

$$\alpha_0' = \int_0^1 \text{coh}(\xi)^{1/2} d\xi \qquad k = 0 \tag{27}$$

We can evaluate Eq. (27) and obtain the values of α_k that will best fit the coherence. If the coherence is an exponential as given in Eq. (24) we can evaluate Eq. (20) and obtain

$$\alpha_0' = 2\xi_0[1 - e^{-1/(\xi_0 2)}]$$

$$\alpha_k' = \frac{4\xi_0[1 - (-1)^k e^{-1/\xi_0 2}]}{[(k2\pi\xi_0)^2 + 1]} \tag{28}$$

We can then write

$$C_0^2 = \alpha_0' \quad 2C^2 = \alpha_1' \quad 2C_2^2 = \alpha_2' \quad \ldots \quad 2C_p^2 = \alpha_p' \tag{29}$$

Then

$$s_p = C_0^2 + 2\sum_{\ell=1}^{p} C_\ell^2 \tag{30}$$

Note that the values of C_i can be multiplied by an arbitrary constant without changing the coherence (Eq. (19)). Evaluating mcoh from Eq. (19) gives the results shown in Fig. 3 for different numbers of noise sources.

The model coherence in Fig. 3 can be seen to decrease with increasing values of $k\Delta$. Thus, as the separation distance Δ or the spatial frequency k increase the coherence decreases. This result is to be expected since as the difference in altitude increases one would expect the wind velocities at the two levels to be increasingly dissimilar, thereby having a lower coherence. Also for the higher frequency, the eddies and integral scales will be smaller thereby giving lower coherence for a given separation distance Δ. It can also be seen that a relatively large number of noises are needed to reduce the model coherence down to that of the measured wind coherence.

It can be seen in Fig. 3 that the model coherence has a zero, continuous slope at $k\Delta$ of 0. The commonly used exponential fit to the experimental data has a nonzero, noncontinuous derivative at $k\Delta$ of 0. It would seem in this case that the model coherence more closely approaches the true situation than the exponential fit since physical systems rarely have discontinuous behavior.

Also shown in Fig. 3 are the vertical velocity component coherence coh_{33} as well as a cross-coherence term coh_{1a} which will be discussed later.

This completes the coherence matching. We next proceed to examine the one-point autospectrum.

B. One-Level Autospectral Density Matching

In this section, we seek to determine the simulation of the one level autospectral function $\phi(k,z,z)$ by the model autospectral function $m\phi(k,z,z)$. From Eqs. (13), (17), and (22) we can see that the two-point autospectrum is given by

$$m\phi(k,z_1,z_2) = A^2 \hat{H}(k,z_1)\hat{H}^*(k,z_2)\left(C_0^2 + 2\sum_{\ell=1}^{p} C_\ell^2 \cos(\pi\ell\xi)\right)$$

Thus the one-point autospectrum at z is

$$m\phi(k,z,z) = A^2 \hat{H}(k,z)\hat{H}^*(k,z)\left(C_0^2 + 2\sum_{\ell=1}^{p} C_\ell^2\right) \tag{31}$$

If we let

$$A^2 = \frac{1}{C_0^2 + 2\sum_{\ell=1}^{p} C_\ell^2} = \frac{1}{s} \tag{32}$$

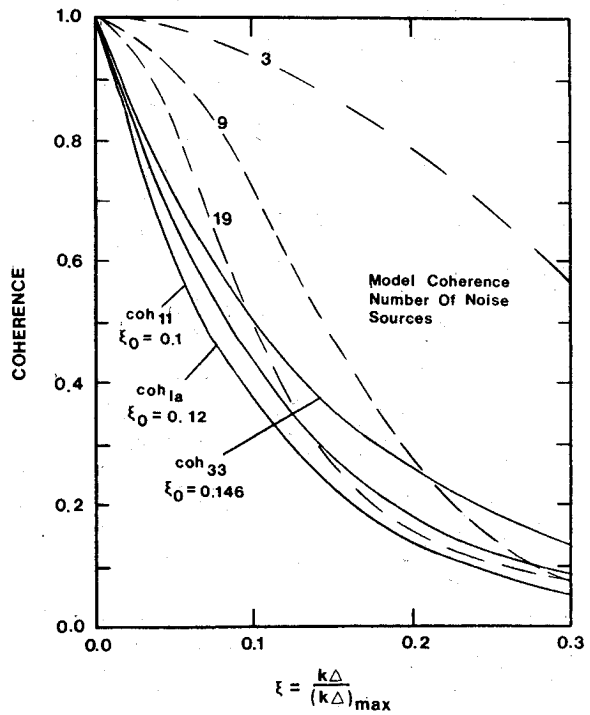

Fig. 3 Wind-turbulence coherence (coh) compared to model coherence (mcoh) for different numbers of noise sources.

we obtain

$$\phi(k,z,z) = \hat{H}(k,z)\hat{H}^*(k,z) \tag{33}$$

where we have equated the model one-level autospectrum $m\phi$ to the one-level autospectrum of the physical turbulence ϕ. Thus if we let

$$\hat{H}(k,z) = \hat{M}(k,z)e^{-i\theta_p(k,z)} \tag{34}$$

we can obtain

$$\hat{M}(k,z) = \phi^{1/2}(k,z,z) \tag{35}$$

The phase angle θ_p will be evaluated in the next section by the requirements on the spectral phase angle θ.

C. Phase-Angle Matching

In this section, we develop the appropriate matching between the model phase angle $m\theta$ and the turbulence phase angle θ. From Eq. (13) we can write the two-level autospectrum in polar form as

$$\begin{aligned} &|m\phi(k,z_j,z_2)|\exp\{-im\theta(k,z_1,z_2)\} \\ &= A^2\hat{M}(k,z_1)\hat{M}(k,z_2)\{\exp -i[\theta_p(k,z_1) \\ &-\theta_p(k,z_2)]\}|\phi_s(k,z_1,z_2)| \end{aligned} \tag{36}$$

Note that, since $\phi_s(k,z_1,z_2)$ is real (see Eqs. (13) and (17)), it therefore has a phase angle of zero.

As will be discussed later, the turbulence two-level autospectral phase angle is usually taken in the form[2]

$$\theta(k,z_1,z_2) = b_{11}k\Delta_{12} \tag{37}$$

where b_{11} is some constant. Setting $m\theta$ equal to θ in Eq. (37) then gives

$$\theta(k,\Delta) = b_{11}k\Delta_{12} = \theta_p(k,z_1) - \theta_p(k,z_2) \tag{38}$$

We can let $\theta_p(k,z_1)$ at some reference level z_1 equal zero then

$$\theta_p(k,z_2) = \theta_p(k\Delta_{12}) = -\theta(k\Delta_{12}) = -b_{11}k\Delta_{12} \tag{39}$$

This concludes the section on matching the two-level autospectrum model to that of wind turbulence.

IV. Transformation to Vehicle Trajectory Turbulence

In the previous section we derived the turbulent frozen field $v(x,z)$. In aerospace applications we desire the turbulent components along some aircraft trajectory $[x_a(t), z_a(t)]$. The x_a and z_a are the horizontal and vertical coordinates of the vehicle at time t. Rather than generate the entire frozen field and then pick out the turbulent components along some trajectory we can transform variables so that the turbulence encountered by the aircraft as a function of time can be calculated directly as follows.

Since we can represent $v(x,z)$ in terms of convolution integrals in real space

$$v(x,z) = \sum_{\ell=-p}^{p} I_\ell(x,z) * N_\ell(x) \tag{40}$$

where I represents the filter

$$I_\ell(x,z) = FT^{-1}[AH(k,z)D_\ell(k,z)] \tag{41}$$

and $N_\ell(x)$ is the white Gaussian noise. Then letting

$$x = \int_0^t V_{a,x}(t)\,dt = x(t) \qquad z = \int_0^t V_{a,z}\,dt = z(t) \tag{42}$$

we would then obtain

$$v(t) = \sum_{\ell=-p}^{p} I_\ell(x(t),z(t)) * N_\ell[x(t)]$$

thereby giving the turbulence incident on an aircraft as a function of time.

V. Gust Statistics

The information needed to implement the simulation scheme is the coherence $\mathrm{coh}_{ij}(k,z_1,z_2)$, the phase angle $\theta_{ij}(k,z_1,z_2)$, and the one-point spectra $\phi_{ij}(k,z,z)$. The following section discusses these functions.

A. One-Point Spectra

For low-altitude turbulence, it is generally accepted that the turbulence is homogeneous in the horizontal plane over a flat terrain, but nonhomogeneous with altitude. The turbulence amplitude and scale therefore tend to vary with altitude.

Although for isotropic turbulence the correlations between orthogonal components must be zero, a nonzero component has been found to exist between the turbulence component in the direction of the mean wind and the turbulence component in the vertical direction, i.e., $\langle(u_1u_3)\rangle \neq 0$. Experimental evidence indicates that the only nonzero correlation between different velocity components at the same point are between the longitudinal and vertical components.[3] As is well known, at high spatial frequencies the turbulence is isotropic. This implies that the cross-spectrum term exists only at low spatial frequencies. It is generally concluded that the cross-spectrum has significant magnitude at frequencies too low to be important to the interaction of aircraft with the turbulent field. At sufficiently high altitudes (generally above 1000 ft) the turbulence can normally be considered isotropic.

In keeping with common practice we shall assume that the isotropic shapes of the spectra hold for the nonisotropic condition at low altitude but that the variance and the integral scale vary. One spectrum form commonly used is the Dryden spectrum given by

$$\phi_{11} = \frac{\sigma_H^2 L_H}{\pi[1+(L_Hk)^2]} \tag{43}$$

$$\phi_{22} = \frac{\sigma_H^2 L_H[1+3(L_Hk)^2]}{2\pi[1+(L_Hk)^2]^2} \tag{44}$$

$$\phi_{33} = \frac{\sigma_v^2 L_v[1+3(L_vk)^2]}{2\pi[1+(L_vk)^2]^2} \tag{45}$$

The σ_H, σ_v are the mean deviations in the horizontal, vertical component and L_H, L_v are the integral scales for the horizontal, vertical component. For level terrain, it was found that the integral scale and the standard deviation for the two horizontal components were equal,[3] i.e., $\sigma_1 = \sigma_2 = \sigma_H$, $L_1 = L_2 = L_H$. The correlations in these cases are

$$R_{11} = \frac{\sigma_H^2}{2\pi}\exp\left(-\left|\frac{r}{L_H}\right|\right) \tag{46}$$

$$R_{22} = \frac{\sigma_H^2}{2\pi}\exp\left(-\left|\frac{r}{L_H}\right|\right)\left(1-\left|\frac{r}{2L_H}\right|\right) \tag{47}$$

and

$$R_{33} = \frac{\sigma_v^2}{2\pi}\exp\left(-\left|\frac{r}{L_V}\right|\right)\left(1-\left|\frac{r}{2L_v}\right|\right) \tag{48}$$

B. Variance and Integral Scale

To determine the standard deviation σ or the integral scale L, we assume, as is commonly done, a neutral atmosphere.

For those applications where the turbulence at the higher altitudes are not too significant, the vertical turbulence standard deviation is given by Ref. 3.

$$\sigma_v = 0.1061\ \bar{v}_{20} \tag{49}$$

where $\bar{v}_{20}$ is the wind velocity in knots at the 20 m level. Typical probable values of $\bar{v}_{20}$ are shown in Fig. 4.

The horizontal standard deviation can be represented by Ref. 3.

$$\sigma_H = \begin{cases} \dfrac{\sigma_v}{[0.177+(0.823\ z/1000)]^{0.4}} & z<1000 \text{ ft} \\ \sigma_v & z>1000 \text{ ft} \end{cases} \tag{50}$$

A plot of σ_H/σ_v is shown in Fig. 5. Since σ_v is constant with altitude, we can see that the horizontal standard deviation σ_H becomes smaller with altitude, implying that the magnitude of the horizontal turbulent fluctuations become smaller with increasing altitude. The vertical scale length is usually assumed to be given by Ref. 3

$$L_v = \begin{cases} z & z<1000 \text{ ft} \\ 1000 & z>1000 \text{ ft} \end{cases} \tag{51}$$

That is, the eddy sizes are assumed to increase with increasing altitude up to 1000 ft. This causes the magnitude in the spectra to move toward smaller k with increasing altitude.

From the condition of local isotropy at low altitudes we can obtain[3]

$$L_H = \begin{cases} \left(\dfrac{\sigma_H}{\sigma_r}\right)^3 L_v = \dfrac{z}{[0.177+0.823(Z/1000)]^{1.2}} & z<1000 \text{ ft} \\ 1000 & z>1000 \text{ ft} \end{cases} \tag{52}$$

These results are shown in Fig. 6.

C. Coherence and Phase Angle

The coherence and phase angle are discussed in Refs. 2 and 4, and the same values will be used here. The values given in Ref. 4 are

$$\mathrm{coh}_{11}(k\Delta) = \exp\left(\frac{-19|k\Delta|}{2\pi}\right) \tag{53a}$$

$$\mathrm{coh}_{22}(k\Delta) = \exp\left(\frac{-13|k\Delta|}{2\pi}\right) \tag{53b}$$

$$\mathrm{coh}_{33}(k\Delta) = \exp\left(\frac{-13|k\Delta|}{2\pi}\right) \tag{53c}$$

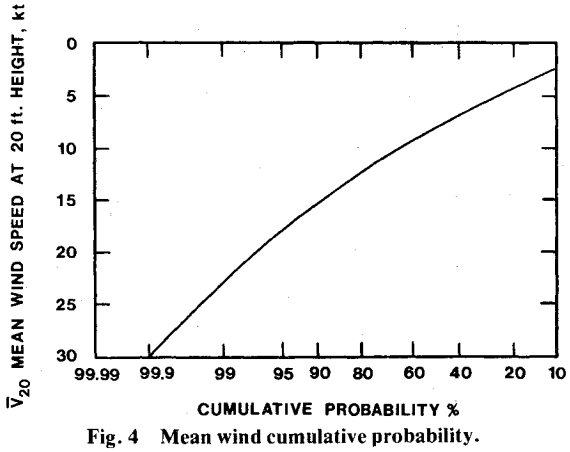

Fig. 4 Mean wind cumulative probability.

and

$$\theta_{11} = k\Delta_{12} \tag{54a}$$

$$\theta_{22} = 2k\Delta_{12} \tag{54b}$$

$$\theta_{33} = 2k\Delta_{12} \tag{54c}$$

where

$$\Delta_{12} = z_1 - z_2$$

VI. Results for Filtering Many White-Noise Inputs

The numerical procedure for generating the wind signal using many independent white-noise inputs can be written as follows. The wind signal at the z_1 level can be written as

$$\hat{v}(k,z_1) = A\hat{M}(k,z_1)\{C_0\hat{N}_0(k) + C_1[e^{ikz_1\pi/\epsilon_0}\hat{N}_1(k) + e^{-ikz_1\pi/\epsilon_0}\hat{N}_{-1}(k)] + C_2[e^{ikz_1 2\pi/\epsilon_0}\hat{N}_2(k) + e^{-ikz_1 2\pi/\epsilon_0}\hat{N}_{-2}(k)]\ldots\} \tag{55}$$

At level z_2, we similarly obtain

$$\hat{v}(k,z_2) = A\hat{M}(k,z_2)e^{ik\Delta_{12}}\{C_0\hat{N}_0(k) + C_1[e^{ikz_2\pi/\epsilon_0}\hat{N}_1(k) + e^{-ikz_2\pi/\epsilon_0}N_{-1}(k)] + C_2[e^{ikz_2 2\pi/\epsilon_0}\hat{N}_2(k) + e^{-ikz_2 2\pi/\epsilon_0}\hat{N}_{-2}(k)]\ldots\} \tag{56}$$

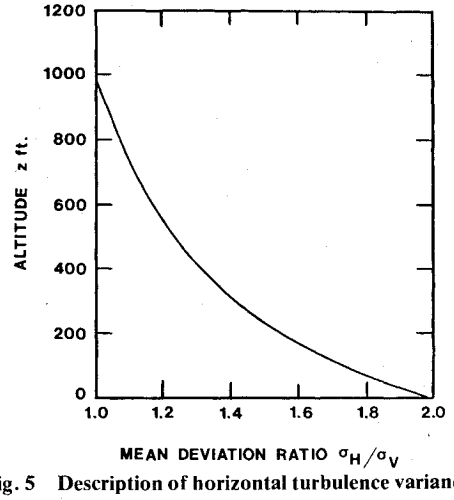

Fig. 5 Description of horizontal turbulence variance.

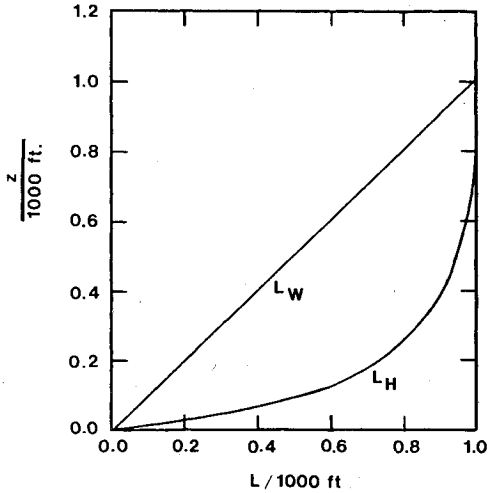

Fig. 6 Integral scale description.

Letting

$$\hat{N}'_1(k)=\hat{N}_1(k)e^{ikz_2\pi/\epsilon_0};$$

$$\hat{N}'_2(k)=\hat{N}_2(k)e^{ikz_2 2\pi/\epsilon_0}$$

$$\hat{N}'_{-1}(k)=\hat{N}_{-1}(k)e^{-ikz_1\pi/\epsilon_0};$$

$$\hat{N}'_{-2}(k)=\hat{N}_{-2}(k)e^{-ikz_1 2\pi/\epsilon_0} \tag{57}$$

Defining

$$\lambda=\Delta_{12}\pi/\epsilon_0 \tag{58}$$

we can then write

$$\hat{v}(k,z_1)=A\hat{M}(k,z_1)\{C_0\hat{N}_0(k)+C_1[e^{ik\lambda}\hat{N}'_1(k)+\hat{N}'_{-1}(k)]+C_2[e^{+ik2\lambda}\hat{N}'_2(k)+\hat{N}'_{-2}(k)]+C_3[e^{ik3\lambda}\hat{N}'_3(k)+\hat{N}'_{-3}(k)]+\ldots\} \tag{59}$$

and

$$\hat{v}(k,z_2)=A\hat{M}(k,z_2)e^{ik\Delta_{12}}\{C_0\hat{N}_0(k)+C_1[\hat{N}'_1(k)+e^{ik\lambda}\hat{N}'_{-1}(k)]+C_2[\hat{N}'_2(k)+e^{ik2\lambda}\hat{N}'_{-2}(k)]+C_3[\hat{N}'_3(k)+e^{ik3\lambda}\hat{N}'_{-3}(k)]+\ldots\} \tag{60}$$

The above can be Fourier transformed to

$$v(x,z_1)=AM(x,z_1)*\{C_0N_0(x)+C_1[N'_1(x+\lambda)+N'_{-1}(x)]+C_2[N'_2(x+2\lambda)+N'_{-2}(x)]+C_3[N'_3(x+3\lambda)+N'_{-3}(x)]+\ldots\} \tag{61}$$

and for z_2

$$v(x,z_2)=v'(x+\Delta_{12},z_2)$$

where

$$v'(x,z_2)=AM(x,z_2)\{C_0N_0(x)+C_1[N'_1(x)+N'_{-1}(x+\lambda)]+C_2[N'_2(x)+N'_{-2}(x+2\lambda)]+C_3[N'_3(x)+N'_{-3}(x+3\lambda)]+\ldots\} \tag{62}$$

Defining the lagged white noise as

$$\tilde{N}_\ell(x)=N'_\ell(x+\ell\lambda) \tag{63}$$

we can then write

$$v(x,z_1)=AM(x,z_1)*\{C_0N_0(x)+C_1[\tilde{N}_1(x)+N'_{-1}(x)]+C_2[\tilde{N}_2(x)+N'_{-2}(x)]+C_3[\tilde{N}_3(x)+N'_{-3}(x)]+\ldots\} \tag{64}$$

and

$$v'(x,z_2)=AM(x,z_2)*\{C_0N_0(x)+C_1[N'_1(x)+\tilde{N}_{-1}(x)]+C_2[N'_2(x)+\tilde{N}_{-2}(x)]+C_3[N'_3(x)+\tilde{N}_{-3}(x)]+\ldots\} \tag{65}$$

Thus, the numerical procedure would be to first generate a Gaussian white noise $N'_\ell(x)$. The lagged noise signal $\tilde{N}_\ell(x)$ can then be obtained by lagging $N'_\ell(x)$. Carrying out this process for the desired total number of noises and summing them with the appropriate constant C_k will give a summed white noise signal. This is digitally convoluted with the shaping filter $M(x,z)$ to give the output wind signal after appropriately lagging $v'(x,z_2)$ as given by Eq. (62). The resulting wind signals are shown in Fig. 7 for 23 noise inputs at levels z_1 and z_2.

In Fig. 8, the one-level autocorrelation signal for the 23 noise cases is shown as triangles. The theoretical results for the autocorrelation does not change with a different number of noise inputs.

In Fig. 9, the two-level autocorrelation results are shown for the 23 noise cases as triangles. Also shown is the theoretical two-level autocorrelation for the wind which from Eq. (8) is given by

$$R(r,z_1,z_2)=FT^{-1}\left\{\left[\hat{M}^2(k,z_1)\hat{M}^2(k,z_2)\times\exp\left(-\frac{19|k\Delta|}{2\pi}\right)\right]^{1/2}e^{-ik\Delta_{12}}\right\}$$

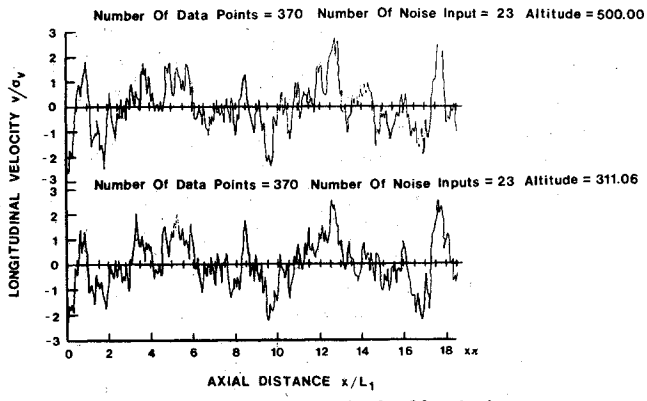

Fig. 7 Longitudinal velocity for 23 noise inputs.

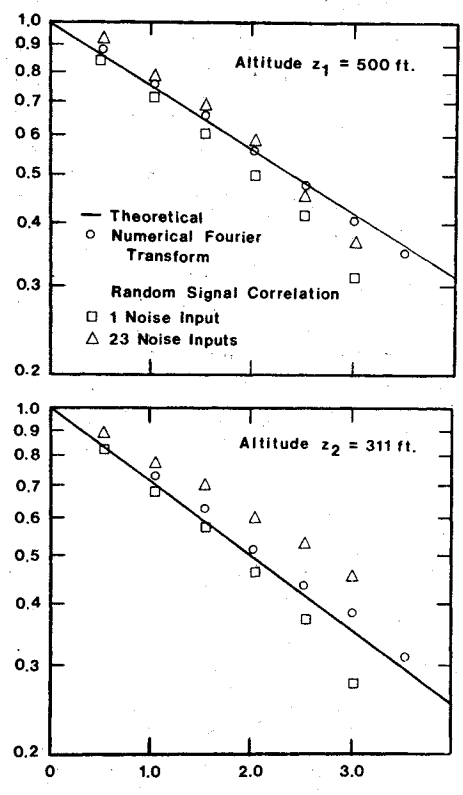

Fig. 8 One-level autocorrelation.

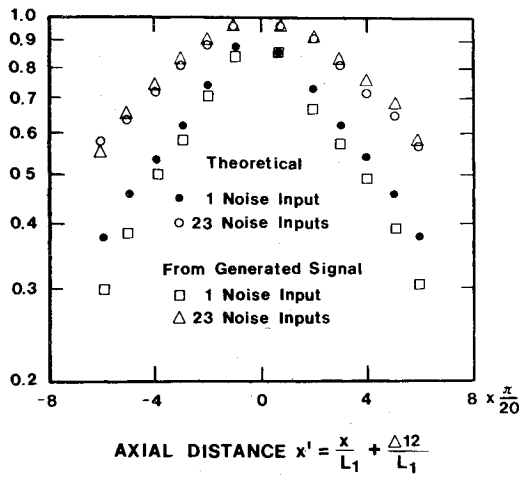

Fig. 9 Two-level autocorrelation.

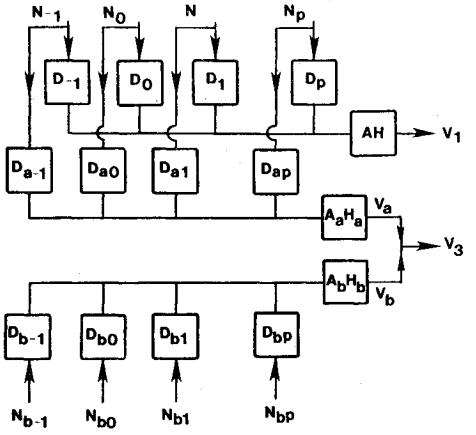

Fig. 10 Control system model for two-velocity-component correlation case.

This was obtained using a numerical inverse Fourier transform as before and is shown as the open circles in Fig. 9. It was found that for nine or more white noises the two-level autocorrelation of the wind model signal falls close to the theoretical wind result.

VII. Cross-Correlation Simulation

In the previous discussion, we assumed that all the cross-spectral terms were negligible. However, this assumption may not always be valid and in some cases it might be necessary to account for the cross spectra in the simulation. Since the only cross-spectrum term that was found to exist was between the longitudinal and the vertical turbulence components $\langle u_1 u_3 \rangle$,[3] the discussion will be restricted to this case, although the method can be applied to all cross-spectrum terms. To simulate u_1, we model v_1 as before (see Fig. 10). The model for v_3 is also shown in this figure. The output signals v_1 and v_3 can be seen from the model to be given by

$$\hat{v}_1(k,z) = AH(z) \sum_{n=-p}^{p} D_n(k,z)\hat{N}_n(k) \tag{66}$$

$$\hat{v}_3(k,z) = A_a H_a(z) \sum_{n=-p}^{p} D_{an}(k,z)\hat{N}_n(k)$$

$$+ A_b H_b(k,z) \sum_{n=-p}^{p} D_{bn}(k,z)\hat{N}_{bn}(k)$$

We can then write the interlevel cross spectrum between v_1 and v_3 as

$$m\phi_{13}(k,z_1,z_2) = AA_a H(k,z_1) H_a^*(k,z_2)$$

$$\times \sum_{n=-p}^{p} D_n(k,z_1) D_{an}^*(k,z_2) = m\phi_{1a}(k,z_1,z_2) \tag{67}$$

where $\langle N_n N_{b,\ell} \rangle = 0$ and $\phi_{N_n N_n} = 1.0$

A. Cross-Coherence Matching

To match the cross coherence we begin by writing the model coherence between output signal v_1 and v_a as

$$\text{mcoh}_{1a}(k,z_1,z_2) = \frac{m\phi_{13}(k,z_1,z_2)\; m\phi_{13}^*(k,z_1,z_2)}{m\phi_{11}(k,z_1,z_1)\; m\phi_{aa}(k,z_2,z_2)} \tag{68}$$

Since $\text{coh}_{13}\ (k,z_1,z_2)$ is the value to be modeled, we can relate mcoh_{13} to mcoh_{1a} by

$$\text{mcoh}_{13}(k,z_1,z_2) = \text{mcoh}_{1a}(k,z_1,z_2)\, \frac{m\phi_{aa}(k,z_2,z_2)}{m\phi_{33}(k,z_2,z_2)} \tag{69}$$

It will be shown later in Eq. (94) that

$$\text{mcoh}_{13}(k,z_1,z_2) = \text{mcoh}_{1a}(k,z_1,z_2)\,\text{mcoh}_{13}(k,z_2,z_2) \tag{70}$$

This shows that the model interlevel cross coherence is a product of two terms: the one-level cross-coherence $\text{mcoh}_{13}(k,z,z)$ and the interlevel cross-coherence factor $\text{mcoh}_{1a}(k,z_1,z_2)$, which is the change in coherence due to changes in separation distance. We can see from Eq. (70) that when $z_1 = z_2$

$$\text{mcoh}_{1a}(k,z_2,z_2) = 1 \tag{71}$$

To find the factor $\text{mcoh}_{1a}(k,z_1,z_2)$ in Eq. (68) the model coherence must equal the turbulent wind coherence, thus from Ref. 4

$$\text{coh}_{1a}(k,z_1,z_2) = \frac{\text{coh}_{13}(k,z_1,z_2)}{\text{coh}_{13}(k,z_2,z_2)} = \exp(-a_a k\Delta) \tag{72}$$

Then we require

$$\text{mcoh}_{1a}(k,z_1,z_2) = \text{coh}_{1a}(k,z_1,z_2) = \exp(-a_a k\Delta) \tag{73}$$

We can write using Eqs. (67) and (68) the result

$$\text{mcoh}_{1a}(k,z_1,z_2) = \frac{\left(\sum_{k=-p}^{p} D_k(k,z_1) D_{ak}^*(k,z_2)\right)}{\left(\sum_{k=-p}^{p} D_k(k,z_1) D_k^*(k,z_1)\right)}$$

$$\times \frac{\left(\sum_{k=-p}^{p} D_k^*(k,z_1) D_{ak}(k,z_2)\right)}{\left(\sum_{k=-p}^{p} D_{ak}(k,z_2) D_{ak}^*(k,z_2)\right)} \tag{74}$$

Notice that the coherence is independent of $A_a H_a$ which can be reserved for the one point cross-spectra and phase angle matching as before. Letting $D_{a\ell}$ be pure leads or lags as we did with D_ℓ in Eq. (16) we can write

$$D_{a\ell} = C_{a\ell}\exp(+ikzd_\ell) \qquad \ell = 1,2,\ldots,p$$

$$D_{a-\ell} = C_{a\ell}\exp(-ikzd_\ell)$$

$$D_{a0} = C_{a0} \tag{75}$$

Then we obtain

$$\sum_{\ell=-p}^{p} D_\ell(k,z_1)D_{a\ell}^*(k,z_2)$$

$$= C_0C_{a0} + \sum_{\ell=1}^{p} C_\ell C_{a\ell}[\exp(-ik\Delta d_\ell) + \exp(ik\Delta d_\ell)] \quad (76a)$$

$$= C_0C_{a0} + 2\sum_{\ell=1}^{p} C_\ell C_{a\ell}\cos(k\Delta d_\ell) \quad (76b)$$

We then can write as in Eq. (19)

$$\text{mcoh}_{1a}(k,z_1,z_2) = \frac{\left(C_0C_{a0} + 2\sum_{\ell=1}^{p} C_\ell C_{a\ell}\cos(k\Delta d_\ell)\right)^2}{\left(C_0C_{a0} + 2\sum_{\ell=1}^{p} C_\ell C_{a\ell}\right)^2} \quad (77)$$

Then, as before

$$\text{mcoh}_{1a}^{1/2}(k,z_1,z_2) = \sum_{\ell=0}^{p} \alpha_{a\ell}\cos\ell\pi\xi$$

where

$$\alpha_{a0} = \frac{C_0C_{a0}}{s_a}, \qquad \alpha_{a1} = \frac{2C_1C_{a1}}{s_a}, \qquad \alpha_{a2} = \frac{2C_2C_{a2}}{s_a} \quad (78)$$

where

$$s_a = C_0C_{a0} + 2\sum_{\ell=1}^{p} C_{a\ell}C_\ell \quad (79)$$

As mentioned previously, the interlevel cross-coherence can be written as [see Eqs. (20) and (73)]

$$\text{coh}_{1a}(k\Delta) = e^{-a_ak\Delta} = e^{-\xi/\xi_a} \quad (80)$$

where

$$\xi_a = 1/a_a\epsilon_0$$

Minimizing as in Eq. (26)

$$E_a = \int_0^1 [\text{mcoh}_{1a}(\xi) - \text{coh}_{1a}^{1/2}(k\Delta)]^2 d\xi \quad (81)$$

Minimizing E_a gives the minimizing values $\alpha'_{a\ell}$, which as in Eq. (29) can be written as

$$\alpha'_{a0} = 2\xi_{a0}[1 - e^{-1/2\xi_{a0}}] \quad (82)$$

$$\alpha'_{a\ell} = 4\xi_{a0}\frac{[1 - (-1)^\ell e^{-1/(2\xi_{a0})}]}{[(\ell\pi 2\xi_{a0})^2 + 1]} \quad (83)$$

We can then write as before in Eq. (30)

$$C_{a0} = \frac{\alpha'_{a0}}{C_0}, \quad 2C_{a1} = \frac{\alpha'_{a1}}{C_1}, \quad 2C_{a2} = \frac{\alpha'_{a2}}{C_2} \ldots \quad (84)$$

where

$$s_a = C_0C_a + 2\sum_{\ell=1}^{p} C_{a\ell}C_\ell$$

Thus we can evaluate C_{a0} to minimize the error E_a.

In Ref. 4 the interlevel cross-coherence factor $\text{coh}_{1a}(k,z_1,z_2)$ is given by

$$\text{coh}_{1a}(k,z_1,z_2) = \exp\left(-16\frac{k\Delta}{2\pi}\right) = \exp(-a_ak\Delta) = \exp(-\xi/\xi_a) \quad (85)$$

By relating the value of ξ_a to the previously used value of $\xi_0 = 0.1$, we have from Eqs. (85) and (53a)

$$\xi_a = \xi_0\left(\frac{a}{a_a}\right) = 0.1\left(\frac{19}{16}\right) = 0.12 \quad (86)$$

Shown in Fig. 3 is a plot of the interlevel cross-coherence factor $\text{coh}_{1a}(k,z_1,z_2)$. We can see that it falls relatively close to $\text{coh}_{11}(k,z_1,z_2)$. This result indicates that for simplicity we could let $C_{ai} = C_i$, which would mean that mcoh_{1a} would be equal to mcoh_{11} as shown in Fig. 3. However, if coh_{1a} was significantly different from coh_{11} then C_{ai} could be evaluated as indicated. It can be seen in the literature that the coherence data have such a wide scatter that the assumption $C_{ai} = C_i$ falls well within the range of experimental data.

B. One-Level Cross-Spectrum Matching

In this section, we seek to simulate the one level cross spectrum, $\phi_{13}(k,z,z)$. We can write from Eqs. (67), (76b), and (79) that when $z_1 = z_2 = z$, the result is

$$m\phi_{13}(k,z,z) = AA_aH(k,z)H_a^*(k,z)s_a \quad (87)$$

Letting

$$A_a = 1/As_a \quad (88)$$

we obtain

$$m\phi_{13}(k,z,z) = H(k,z)H_a^*(k,z) \quad (89)$$

Letting, as in Eq. (35)

$$H_a(k,z) = \hat{M}_a(k,z)e^{-i\theta_a(k,z)} \quad (90)$$

we can obtain

$$\text{m}\phi_{13}(k,z,z)\,m\phi_{13}^*(k,z,z) = \hat{M}^2(k,z)\hat{M}_a^2(k,z) \quad (91)$$

We can then write

$$\hat{M}_a^2(k,z) = m\phi_{aa}(k,z,z) = \frac{m\phi_{13}(k,z,z)\,m\phi_{13}^*(k,z,z)}{m\phi_{11}(k,z,z)} \quad (92)$$

making the model spectra equal to wind spectra then allows us to evaluate $\hat{M}_a(k,z)$ using

$$\hat{M}_a^2(k,z) = m\phi_{aa}(k,z,z) = \frac{\phi_{13}(k,z,z)\phi_{13}^*(k,z,z)}{\phi_{11}(k,z,z)}$$

$$= \text{coh}_{13}(k,z,z)\phi_{33}(k,z,z) \quad (93)$$

This also gives the relationship used earlier in Eq. (69). We can see the spectrum $m\phi_{aa}$ is directly related to the one-level cross coherence. Notice that if $\text{coh}_{13}(k,z,z) = 0$ then $m\phi_{aa}$ would equal zero implying that v_a equal zero and the connective element in Fig. 10 will not exist and the figure becomes similar to Fig. 2 which is the uncorrelated case.

C. Cross-Phase Angle Matching

As before, we can write the model cross-phase angle from Eq. (67) between arbitrary levels z_2 and z_3 as

$$m\theta_{13}(k,z_2,z_3) = \theta_p(k,z_2) - \theta_a(k,z_3) = -\theta_{11}(k\Delta_{21}) - \theta_a(k,z_3) \quad (94)$$

where $\theta_p(k,z_2) = -\theta_{11}(k\Delta_{21})$ has been derived in Eq. (39) and $\Delta_{21} = z_2 - z_1$. Since the quad-spectrum of the one-level cross spectrum is generally considered negligible,[3] we can

assume that θ_{13} will only have an interlevel effect and as shown in Ref. 4 can be written in the form

$$\theta_{13}(k,z_2,z_3)=b_{13}k\Delta_{32} \tag{95}$$

where $\Delta_{32}=z_3-z_2$. We must now evaluate θ_a so as to satisfy Eqs. (94). We can write, using Eqs. (94) and (39)

$$\theta_a(k,z_3)=-\theta_{11}(k\Delta_{21})-\theta_{13}(k\Delta_{32})$$

$$\theta_a(k\Delta_{31})=-b_{11}k\Delta_{21}-b_{13}k\Delta_{32} \tag{96}$$

Since θ_a must only depend on separation distances Δ_{31}, by letting $b_{11}=b_{13}$, we then obtain

$$\theta_a(k\Delta_{31})=-b_{11}k\Delta_{31} \tag{97}$$

Note that for the present model it is required that the cross-phase angle $\theta_{13}(k,z_2,z_3)$ is equal to the longitudinal velocity-phase angle $\theta_{11}(k,z_2,z_3)$ for the case where the cross coherence is important. It is pointed out in the literature[7] that only very little data which scatters over a significant range exists on phase angles so this assumption is not unreasonable.

This concludes the section on matching two level cross spectra between the model and the wind turbulence. We must now satisfy the vertical wind component interlevel autospectrum.

VIII. Vertical Velocity Two-Point Autospectrum Simulation for Cross-Correlation Case

We must now satisfy the vertical velocity two point autospectrum for the cross-correlated case. From the model in Fig. 10, it can be seeen that the $m\phi_{33}(k,z_1,z_2)$ is given by

$$m\phi_{33}(k,z_1,z_2)=A_a^2H_a(z_1)H_a^*(z_2)\sum_{n=-p}^{p}D_{an}(z_1)D_{an}^*(z_2)$$

$$+A_b^2H_b(z_1)H_b^*(z_2)\sum_{\ell=-p}^{p}D_{b\ell}(z_1)D_{b\ell}^*(z_2)$$

$$=m\phi_{aa}(k,z_1,z_2)+m\phi_{bb}(k,z_1,z_2) \tag{98}$$

Since we require the wind two-point autospectral to be equal to that of the model

$$\phi_{33}(k,z_1,z_2)=m\phi_{33}(k,z_1,z_2) \tag{99}$$

Also since $m\phi_{aa}$ is known from the previous section, we can write

$$m\phi_{bb}(k,z_1,z_2)=\phi_{33}(k,z_1,z_2)-m\phi_{aa}(k,z_1,z_2) \tag{100}$$

Thus one method for simulating u_3 would be to solve for A_b, D_{bm}, and H_b as described in the previous Sec. III for the case where the autospectrum would be given by $m\phi_{bb}$. One procedure for simulating v_b is as follows. In Eq. (66), v_3 was given as

$$\hat{v}_3(k,z)=A_aH_a(k,z)\sum_{n=-p}^{p}D_{an}(k,z)\hat{N}_n(k)$$

$$+A_bH_b(k,z)\sum_{n=-p}^{p}D_{bn}(k,z)\hat{N}_{bn}(k) \tag{101}$$

Let us assume that

$$f_a(k)H_3(k,z)=H_a(k,z)$$

$$f_b(k)H_3(k,z)=H_b(k,z) \tag{102}$$

where $f_a(k)$ and $f_b(k)$ are real functions of k that change slowly with z, are considered quasiconstant over z, and will be defined more fully later. We can now write

$$\hat{v}_3(k,z)=H_3(k,z)\left[A_af_a(k)\sum_{n=-p}^{p}D_{an}(k,z)N_n(k)\right.$$

$$\left.+A_bf_b(k)\sum_{n=-p}^{p}D_{bn}(k,z)N_{bn}(k)\right] \tag{103}$$

We can write the two level autospectrum as

$$m\phi_{33}(k,z_1,z_2)=H_3(k,z_1)H_3^*(k,z_2)\left[A_a^2f_a^2(k)\sum_{n=-p}^{p}D_{an}(k,z_1)\right.$$

$$\left.D_{an}^*(k,z_2)+A_b^2f_b^2(k)\sum_{n=-p}^{p}D_{bn}(k,z_1)D_{bn}^*(k,z_2)\right] \tag{104}$$

Assuming as before

$$D_{b\ell}=C_{b\ell}\exp(ikzd_\ell)\qquad \ell=1,2,\ldots \tag{105}$$

$$D_{b-\ell}=C_{b\ell}\exp(-ikzd_\ell)$$

$$D_{b0}=C_{b0}$$

we can write Eq. (104) as (as in Eq. 17)

$$m\phi_{33}(k,z_1,z_2)=H_3(k,z_1)H_3^*(k,z_2)$$

$$\left\{A_a^2f_a^2(k)\left[C_a^2+2\sum_{\ell=1}^{p}C_{a\ell}^2\cos(k\Delta d_\ell)\right]\right.$$

$$\left.+A_b^2f_b^2(k)\left[C_b^2+2\sum_{\ell=1}^{p}C_{b\ell}^2\cos(k\Delta d_\ell)\right]\right\} \tag{106}$$

A. Coherence Matching for Vertical Component

The two-point autocoherence is now given by

$$\mathrm{mcoh}_{33}(k,z_1,z_2)$$

$$=\frac{H_3(z_1)H_3^*(z_2)H_3^*(z_1)H_3(z_2)}{H_3(z_1)H_3^*(z_1)H_3(z_2)H_3^*(z_2)}\times\frac{\left(\left\{A_a^2f_a^2(k)\left[C_a^2+2\sum_{\ell=1}^{p}C_{a\ell}^2\cos(k\Delta d_\ell)\right]\right\}+\left\{A_b^2f_b^2(k)\left[C_b^2+2\sum_{\ell=1}^{p}C_{b\ell}\cos(k\Delta d_\ell)\right]\right\}\right)^2}{\left\{\left[A_a^2f_a^2(k)\left(C_a^2+2\sum_{\ell=1}^{p}C_{a\ell}\right)\right]+\left[A_b^2f_b^2(k)\left(C_b^2+2\sum_{\ell=1}^{p}C_{b\ell}^2\right)\right]\right\}^2} \tag{107}$$

This can be simplified greatly if we let

$$A_a^2C_{a\ell}^2=A_b^2C_{b\ell}^2 \tag{108}$$

then Eq. (107) reduces to

$$\mathrm{mcoh}_{33}^{1/2}(k,z_1,z_2)=\frac{\left(C_{0a}^2+2\sum_{\ell=1}^{p}C_{a\ell}\cos k\Delta d_\ell\right)}{\left(C_{0a}^2+2\sum_{\ell=1}^{p}C_{a\ell}^2\right)} \tag{109}$$

This can readily be evaluated using the values of $C_{a\ell}$ found previously. If we assume $C_{a\ell}=C_\ell$, then we obtain

$$\mathrm{mcoh}_{33}^{1/2}(k,z_1,z_2)=\mathrm{mcoh}_{11}^{1/2}(k,z_1,z_2) \tag{110}$$

From Eq. (53c), we can write as in Eq. (85)

$$\mathrm{coh}_{33}(k\Delta) = \exp\left(-\frac{13k\Delta}{2\pi}\right) = \exp(-a_3 k\Delta) = \exp(-\xi/\xi_3)$$

Relating ξ_3 to ξ_0, we can, as in Eq. (86), write

$$\xi_3 = \xi_0\left(\frac{a}{a_3}\right) = 0.1\left(\frac{19}{13}\right) = 0.146$$

Figure 3 shows a plot of $\mathrm{coh}_{33}(k,z_1,z_2)$. We see that it falls relatively close to $\mathrm{coh}_{11}(k,z_1,z_2)$; therefore, Eq. (110) is not an unreasonable assumption considering the scatter in the experimental data.[7]

B. One-Level Autospectral Matching

The one-level autospectrum from Eq. (104) can be written as

$$m\phi_{33}(k,z,z) = H_3(k,z)H_3^*(k,z)\left[A^2\left(C_0^2 + 2\sum_{\ell=1}^{p} C_\ell^2\right)\right][f_a^2(k) + f_b^2(k)] = H_3(k,z)H_3^*(k,z)[f_a^2(k) + f_b^2(k)] \quad (111)$$

Using Eq. (102), this becomes

$$m\phi_{33}(k,z,z) = H_a(k,z)H_a^*(k,z) + H_b(k,z)H_b^*(k,z) \quad (112)$$

$$= m\phi_{aa}(k,z,z) + m\phi_{bb}(k,z,z) \quad (113)$$

We can see from Eq. (102) that

$$f_a^2(k) = \frac{m\phi_{aa}(k,z,z)}{m\phi_{33}(k,z,z)} \qquad f_b^2(k) = \frac{m\phi_{bb}(k,z,z)}{m\phi_{33}(k,z,z)} \quad (114)$$

From Eq. (113)

$$f_a^2(k) + f_b^2(k) = 1$$

Recalling Eq. (93) we obtain

$$f_a^2(k) = \mathrm{coh}_{13}(k,z,z) \quad (115)$$

This allows evaluation of $f_a^2(k)$. We have assumed $f_a(k)$ varies slowly in z so that the change in $f_a^2(k)$ is not significant over the range $(k\Delta)_{\max}$. If $\mathrm{coh}_{13}(k,z,z)$ is zero then f_a would be zero. This gives $H_a = 0$ and $m\phi_{bb}(k,z,z) = \phi_{33}(k,z,z)$, and the model reduces to the uncorrelated case.

As before we can write

$$H_b(k,z) = \hat{M}_b(k,z)e^{-i\theta_b(k,z)} \quad (116)$$

Then we can evaluate $\hat{M}_b$ from

$$\hat{M}_b(k,z) = \{\phi_{33}(k,z,z) - m\phi_{aa}(k,z,z)\}^{1/2} = \{\phi_{33}(k,z,z)[1 - \mathrm{coh}_{13}(k,z,z)]\}^{1/2} \quad (117)$$

C. Phase Angle Matching

To develop the appropriate matching between the model phase angle $m\theta_{33}$ and the turbulence phase angle θ_{33} we can write from Eq. (106)

$$m\theta_{33}(k,z_3,z_3) = \theta_3(k,z_2) - \theta_3(k,z_3) \quad (118)$$

Thus we can write

$$\theta_3(k\Delta_{32}) = -\theta_{33}(k\Delta_{32}) \quad (119)$$

Since

$$f_a(k)H_3(k,z) = H_a(k,z)$$

and

$$f_b(k)H_3(k,z) = H_b(k,z)$$

$$\theta_3(k\Delta) = \theta_b(k\Delta) = \theta_a(k\Delta) = \theta(k\Delta) = -b_{11}(k\Delta) \quad (120)$$

Thus for the present model, the phase angles for the vertical component θ_{33} must be equal to the phase angle for the longitudinal component θ_{11}. As pointed out previously, as shown in Ref. 7, the scatter in the turbulent phase angle data is sufficiently large that refinement of this assumption is unjustified.

IV. Conclusions

A method has been presented for modeling the three components of the atmospheric wind turbulence in a vertical plane so that the second moment turbulent wind statistics are satisfied. The method is sufficiently general so that a wide range of coherences, spectra, and phase angles can be incorporated that would allow simulation of a wide rnage of different atmospheric conditions to be modeled.

Since the wind components are given in functional form, various other quantities of interest such as wind derivatives or probability distributions of turbulent wind amplitudes can readily be obtained.

The random turbulent field can be generated numerically either as wind field impinging on an aircraft, balloon, a wind power generator, or building as a function of time or as a random frozen turbulent field. These numerical calculations would allow strongly nonlinear interactions between the turbulent random field and an aircraft to be calculated numerically. This would be difficult to achieve using more conventional linear analytic techniques.

The present model depends strongly on the availability of good statistical wind data. The need for better coherence, spectral and phase angle information for various atmospheric conditions is indicated. This data would also be useful in refining the present model or developing improved models.

The present method is not restricted to wind simulation but is applicable to other problems related to multicomponent multidimensional random fields.

Various possible extensions of the present analysis exist. The present technique can be extended from a vertical turbulent plane to a three-dimensional turbulent field. This would allow more general wind turbulence-aircraft interactions to be solved. Another interesting extension would be to consider the case when, due to rough terrain or buildings, the wind is no longer horizontally stationary.

References

[1] Frost, W. and Moulden, T., *Fundamentals and Applications of Turbulence*, Plenum Press, New York, 1977.

[2] Fichtl, G. H. and Perlmutter, M., "Nonstationary Atmospheric Boundary-Layer Turbulence Simulation," *Journal of Aircraft*, Vol. 12, Aug. 1975, pp. 639-647.

[3] Barr, N. M., Gangaas, D., and Schaeffer, D. R., "Wind Models for Flight Simulation Certification of Landing and Approach Guidance and Control Systems," FAA-RD-74-206, Dec. 1974.

[4] Sinha, A. K., "On Digital Simulation of Multicorrelated Random Processes and its Applications," Virginia Polytechnic Institute and State University, July 1973.

[5] Perlmutter, M., "Three Velocity Component Nonhomogeneous Atmosphere Boundary-Layer Turbulence Modeling," University of Tennessee, Knoxville, Aug. 1976.

[6] Bendat, J. S. and Piersol, A. G., *Random Data: Analysis and Measurement Procedures*, Wiley-Interscience, New York, 1971.

[7] Dutton, J. A., Panofsky, H. A., Deaven, D. C., Kerman, B. R., and Mirabella, V., "Statistical Properties of Turbulence at the Kennedy Space Center for Aerospace Vehicle Design," NASA CR-1889, Aug. 1971.